

HYBRID EQUILIBRIUM FINITE ELEMENTS FOR WAVE DIFFRACTION PROBLEMS

Z. M. Wang¹, M. L. Peterson¹, and Ya. M. Grigorenko²

UDC 539.3

Hybrid equilibrium finite elements based on the direct approximation of the domain stress and boundary displacement fields are presented. The structure is divided into a far field, which is considered as an infinite super element, and a near field, which is in turn discretized into finite elements. The displacements in the domains of typical finite elements are obtained from the assumed domain stress field by using the dynamic equilibrium equations. The Helmholtz equation is satisfied in the domain of the infinite super element, and the domain stress fields are associated with elastic and compatible displacements. The resulting governing system is symmetric, sparse, and, if well done, positive. Numerical applications are presented to illustrate the performance of the formulation.

Keywords: hybrid equilibrium finite elements, far field, near field, wave diffraction problem, Helmholtz equation, resulting governing system

1. Introduction. Wave diffraction problems are usually formulated in unbounded domains wherein the waves are governed by the Helmholtz equation and the scattered components of the waves are subject to the Sommerfeld radiation condition at infinity. Such exterior wave problems have been solved by a number of numerical methods. Among these methods are the infinite-element method (IEM) [1–5], which is based on the Helmholtz differential equation and a field variable represented by a trial function over an entire semi-infinite sector of space, and the boundary-element method (BEM) [6–9], which is based on the surface Helmholtz integral equation applied to the surface of the structure.

The present paper explores a hybrid equilibrium finite element in which the stresses in the domain of the element and the displacements on its boundary are independently approximated and in which the approximations in the domain are constrained to locally satisfy the equilibrium equations. Pioneering applications of the hybrid equilibrium elements are proposed by Pian [10], Pian and Tong [11], Atluri [12], Cook and Ladkany [13], in which the optimum of assumed stress distributions is pursued and elementary systems are condensed into a reduced number of freedom used for conforming nodal displacement fields before assembling. Recently, in the development of hybrid equilibrium elements, Jirousek and Wroblewski [14], Almeida and Pereira [15], Freitas and Ji [16], Freitas and Wang [17], and Pereira, Almeida, and Maunder [18] emphasized the use of generalized variables and of high-degree and naturally hierarchical bases implemented on coarse meshes of macro- and super-elements instead of insisting on using concepts, techniques, and tools directly imported from the experience accumulated with the conforming displacement elements. Particularly, when the Trefftz constraints that all of the equations are locally satisfied in the domains are imposed on the assumed stress fields, all the intervening structural matrices and vectors have boundary integral expressions, a typical characteristic of the boundary-element method. More recently, Freitas [19], Freitas and Wang [20], and Freitas and Wang [21] extended the hybrid equilibrium elements to elastodynamic problems, whose characteristic feature in the FE analyses is that the displacements in the domains are derived from the assumed stress distributions by using the dynamic equilibrium equations.

¹University of Maine, Orono, ME 04469, USA. ²S. P. Timoshenko Institute of Mechanics, National Academy of Sciences of Ukraine, Kiev. Published in *Prikladnaya Mekhanika*, Vol. 39, No. 9, pp. 135–144, September 2003. Original article submitted November 14, 2002.

Grigorenko and Kokoshin [22, 23] used the hybrid model of the finite-element method based on the mixed Reissner variational principle to design shell structures. Some aspects of different applications of the finite-element method are addressed in [24–26].

In the present paper, hybrid elements are applied to the wave diffraction problem. The structure is divided into a far field, which is considered as an infinite super element, and a near field, which is in turn discretized into finite elements. In a typical element in the near field, unconstrained polynomials are used as approximation functions, while the Hankel function of the first kind is adopted to satisfy the Helmholtz differential equation in the domain of the infinite element and the Sommerfeld radiation condition at infinity. Conditions that are not satisfied locally are enforced in the Galerkin weighed residual form so designed as to ensure energy equivalence. The resulting governing system is symmetric and sparse. It is intended to be solved by a sufficient code suitable for large sparse systems. As the Helmholtz differential equation in the domain of the infinite element is locally satisfied, the intervening structural matrices and vectors concerning infinite fields have much simpler boundary integral expressions.

This paper is organized in the following manner. The fundamental equations are presented first. Hybrid element approximation criteria are then set up and finite element formulations are derived by the weighed residual enforcement of the fundamental conditions. Finally, two tests are performed to verify the effectiveness of the finite-element method.

2. Fundamental Equations. Let V represent the domain of an element and Γ , the enveloping surface, referred to a Cartesian system x , and t define a time parameter. The fundamental equations governing linear elastodynamic problems are

$$\mathbf{D}\boldsymbol{\sigma}(\mathbf{x}, t) = \rho \ddot{\mathbf{u}}(\mathbf{x}, t) \quad \text{in } V, \quad (1)$$

$$\boldsymbol{\varepsilon}(\mathbf{x}, t) = \mathbf{D}^* \mathbf{u}(\mathbf{x}, t) \quad \text{in } V, \quad (2)$$

$$\boldsymbol{\varepsilon}(\mathbf{x}, t) = \mathbf{D}\boldsymbol{\sigma}(\mathbf{x}, t) \quad \text{in } V, \quad (3)$$

$$\mathbf{n}\boldsymbol{\sigma}(\mathbf{x}, t) = \mathbf{t}_\Gamma(\mathbf{x}, t) \quad \text{on } \Gamma_\sigma, \quad (4)$$

$$\mathbf{u}(\mathbf{x}, t) = \mathbf{u}_\Gamma(\mathbf{x}, t) \quad \text{on } \Gamma_u, \quad (5)$$

$$\mathbf{u}(\mathbf{x}) = \mathbf{u}_0(\mathbf{x}) \quad \text{in } V, \quad (6)$$

$$\dot{\mathbf{u}}(\mathbf{x}) = \dot{\mathbf{u}}_0(\mathbf{x}) \quad \text{in } V. \quad (7)$$

In the equations of dynamic equilibrium, compatibility and elasticity relations (1), (2), and (3), the vectors \mathbf{u} , $\boldsymbol{\varepsilon}$ and $\boldsymbol{\sigma}$ collect the components of the displacement, strain, and stress tensors, respectively, and ρ and the matrix \mathbf{f} are the mass density and elastic constants, respectively. Since a geometrically linear model is assumed, the differential equilibrium and compatibility operators \mathbf{D} and \mathbf{D}^* are linear and adjoint.

Equations (4) and (5) are referred to static and kinematic boundary conditions on the complementary portions Γ_σ and Γ_u , respectively. In Eq. (4), \mathbf{n} collects the components of the unit outward normal vector. Equations (6) and (7) define the initial conditions for displacements and velocity, respectively.

The steady-state solution of the problem for a general variable is

$$\mathbf{v}(\mathbf{x}, t) = \mathbf{v}(\mathbf{x}, t) e^{i\omega t}. \quad (8)$$

Thus, Eqs. (1–7) can be written in the following form:

$$\mathbf{D}\boldsymbol{\sigma}(\mathbf{x}) = -\rho\omega^2 \mathbf{u}(\mathbf{x}) \quad \text{in } V, \quad (9)$$

$$\boldsymbol{\varepsilon}(\mathbf{x}) = \mathbf{D}^* \mathbf{u}(\mathbf{x}) \quad \text{in } V, \quad (10)$$

$$\boldsymbol{\varepsilon}(\mathbf{x}) = \mathbf{f}\boldsymbol{\sigma}(\mathbf{x}) \quad \text{in } V, \quad (11)$$

$$\mathbf{n}\boldsymbol{\sigma}(\mathbf{x}) = \mathbf{t}_\Gamma(\mathbf{x}) \quad \text{on } \Gamma_\sigma, \quad (12)$$

$$\mathbf{u}(\mathbf{x}) = \mathbf{u}_\Gamma(\mathbf{x}) \quad \text{on } \Gamma_u. \quad (13)$$

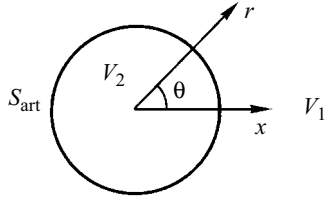


Fig. 1. Artificial circular boundary between infinite element and finite elements

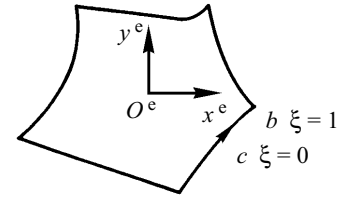


Fig. 2. A typical element and its boundary

All the equations below will be referred to as those in the steady-state fields; and the Cartesian system x will be omitted for simplicity.

3. Finite Element Approximation Bases. The hybrid equilibrium model adopted is based on the direct approximation of the stresses in the domain of the element and of the displacements on its static boundary, which is the union of the element boundaries whereon displacements are not specified:

$$\sigma = \mathbf{S}_v \mathbf{p} + \sigma_{\text{inc}} \quad \text{in } V, \quad (14)$$

$$\mathbf{u} = \mathbf{Z} \mathbf{q} \quad \text{in } \Gamma_\sigma, \quad (15)$$

where \mathbf{S}_v and \mathbf{Z} collect, as columns, the domain scattered stress and boundary displacement approximation functions, respectively, \mathbf{p} and \mathbf{q} are vectors that list the associated parametric weights, and σ_{inc} and \mathbf{u}_{inc} are the domain incident stresses and displacements, respectively, which satisfy the domain equations (9)–(11), namely the Trefftz constraints. The associated domain displacement fields can be written in the following form:

$$\mathbf{u}_v = \mathbf{U}_v \mathbf{p} + \mathbf{u}_{\text{inc}} \quad \text{on } V, \quad (16)$$

where the matrix \mathbf{U}_v , associated with the matrix \mathbf{S}_v , collects the domain scattered displacement approximation functions.

In Fig. 1, the artificial circle \mathbf{S}_{art} is large enough to surround all geometric and material irregularities, V_1 is the region exterior to the artificial circle, which represents the infinite super element, and V_2 is the interior region of the artificial circle, which is divided into finite elements.

In the domain of a typical finite element inside the artificial circle in Fig. 2, the stress approximation functions associated with the scattered wave may be expressed in local cantilever coordinates as follows:

$$\mathbf{S}_v = \begin{bmatrix} P_1 & 0 & 0 \\ 0 & P_1 & 0 \\ 0 & 0 & P_1 \end{bmatrix}, \quad (17)$$

where

$$\mathbf{P}_1 = \{1 \ x \ y \ x^2 \ xy \ y^2 \ \dots \ x^m \ x^{m-1} \ y \ \dots \ y^m \}. \quad (18)$$

Thus, the domain displacement approximation functions can be obtained by using the equilibrium equation (9):

$$\mathbf{U}_v = \frac{1}{\rho \omega^2} \mathbf{D} \mathbf{S}_v. \quad (19)$$

For the infinite super element, shown in Fig. 1, the Helmholtz potentials associated with the scattered wave may be written in polar coordinates (r, θ) as follows:

$$\Phi = \{H_0^{(1)}(k_1 r) H_1^{(1)}(k_1 r) \cos \theta H_1^{(1)}(k_1 r) \sin \theta \dots H_n^{(1)}(k_1 r) \cos n\theta H_n^{(1)}(k_1 r) \sin n\theta \}, \quad (20)$$

$$\Psi = \{H_0^{(1)}(k_2 r) H_1^{(1)}(k_2 r) \cos \theta H_1^{(1)}(k_2 r) \sin \theta \dots H_n^{(1)}(k_2 r) \cos n\theta H_n^{(1)}(k_2 r) \sin n\theta \}, \quad (21)$$

where k_1 and k_2 are two ordinary wave numbers and $H_i^{(1)}$ is the Hankel function of the first kind. The scattered wave must die out at infinity; therefore, the Hankel function of the first kind is adopted in the above expressions.

Consequently, the associated displacement and stress approximation bases satisfy the domain equations (9)–(11) and are written in the following form:

$$\mathbf{U}_v = \nabla\Phi + \nabla \times (\mathbf{i}_z \Psi) \quad \text{in } V, \quad (22)$$

$$\mathbf{S}_v = \mathbf{f}^{-1}(\mathbf{D}^* \mathbf{U}_v) \quad \text{in } V. \quad (23)$$

As shown in Fig. 2, polynomials in local coordinate system $-1 \leq \xi \leq 1$ are used to set up the boundary displacement interpolation matrix as follows:

$$\mathbf{Z} = \begin{bmatrix} P_2 & 0 \\ 0 & P_2 \end{bmatrix}, \quad (24)$$

where

$$\mathbf{P}_2 = \{(1-\xi)/2 \quad (1+\xi)/2 \quad 1-\xi^2 \xi(1-\xi^2) \dots\}. \quad (25)$$

In (25), the linear standard functions associated with node values are given in the first two entries and a series of polynomials are always designed to have zero values at the nodes.

4. Finite-Element Formulations. The finite-element approximation bases stated above show that the logic behind the equilibrium model consists, essentially, in the local enforcement of the fundamental conditions characterizing the boundary-value problem under analysis. The conditions that are not satisfied locally by the supporting approximation are enforced in the Galerkin weighted residual form. In a typical element inside the artificial circle, the compatibility condition (10) is enforced by using the stress approximation functions as weighting functions:

$$\int \mathbf{S}_v^t (\boldsymbol{\varepsilon} - \mathbf{D}^* \mathbf{u}) dV = 0, \quad (26)$$

which is integrated by parts to yield

$$\int [\mathbf{S}_v^t \boldsymbol{\varepsilon} + (\mathbf{D}\mathbf{S}_v)^t \mathbf{u}_v] dV - \int (\mathbf{n}\mathbf{S}_v)^t \mathbf{u} d\Gamma = 0, \quad (27)$$

where $\boldsymbol{\varepsilon}$ and \mathbf{u}_v can be obtained from the assumed stress form (14) by using the elasticity relation (11) and Eq. (16), respectively, and the boundary displacements \mathbf{u} are the union of the prescribed boundary displacements \mathbf{u}_Γ in the boundary condition (13) and assumed boundary displacements in the approximation (15). The appropriate combination of Eqs. (27), (14), (11), (16), (19), (13), and (15) and, additionally, the compatibility equation (10) and Green's theorem for the incident wave fields yield

$$(\mathbf{F} - \omega^{-2} \mathbf{M}) \mathbf{p} - \mathbf{A} \mathbf{q} = \mathbf{e}, \quad (28)$$

where

$$\mathbf{F} = \int \mathbf{S}_v^t \mathbf{f} \mathbf{S}_v dV, \quad (29)$$

$$\mathbf{M} = \frac{1}{\rho} \int (\mathbf{D}\mathbf{S}_v)^t \mathbf{D}\mathbf{S}_v dV, \quad (30)$$

$$\mathbf{A} = \int_{\Gamma_G} (\mathbf{n}\mathbf{S}_v)^t \mathbf{Z} ds, \quad (31)$$

$$\mathbf{e} = \int_{\Gamma_u} (\mathbf{n}\mathbf{S}_v)^t \mathbf{u}_\Gamma ds - \int_{\Gamma_u} (\mathbf{n}\mathbf{S}_v)^t \mathbf{u}_{inc} ds. \quad (32)$$

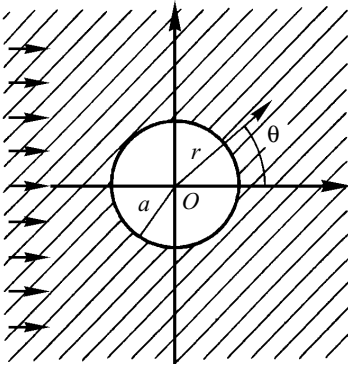
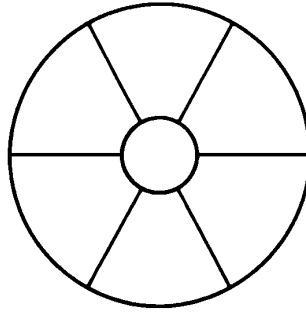
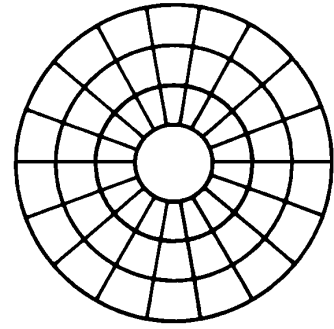


Fig. 3. Infinite plate with a circular cavity



a (6 elements)



b (54 elements)

Fig. 4. Hybrid finite element meshes

In the infinite super element, the Helmholtz differential equation is locally satisfied in the domain and the Sommerfeld radiation condition holds at infinity. Thus, the boundary condition (13) is enforced by using the boundary traction approximation functions as weighting functions:

$$\int_{\text{ort}_u} (\mathbf{nS}_v)^t (\mathbf{u}_v - \mathbf{u}) ds = 0, \quad (33)$$

where the vectors \mathbf{u}_v and \mathbf{u} are the domain and assumed boundary displacements, respectively.

The substitution of (15) and (16) into (33) yields Eq. (28), where the following expressions hold:

$$\mathbf{F} - \omega^2 \mathbf{M} = \int_{\Gamma_{\text{ort}}} (\mathbf{nS}_v)^t \mathbf{U}_v ds, \quad (34)$$

$$\mathbf{e} = \int_{\Gamma_{\text{ort}}} (\mathbf{nS}_v)^t \mathbf{u}_{\text{inc}} ds. \quad (35)$$

Since the equilibrium equation (9) is locally satisfied in the domain of each element, the associated finite element equilibrium condition represents the \mathbf{Z} -weighed residual enforcement of the static boundary condition (12):

$$\int_{\Gamma_{\sigma}} \mathbf{Z}^t (\mathbf{n}\boldsymbol{\sigma} - \mathbf{t}_{\Gamma})^t ds = 0. \quad (36)$$

The substitution of (14) into Eq. (36) produces the following estimates:

$$-\mathbf{A}^t \mathbf{p} = \mathbf{v}, \quad (37)$$

where

$$\mathbf{v} = \int_{\Gamma_{\sigma}} \mathbf{Z}^t (\mathbf{n}\boldsymbol{\sigma}_{\text{inc}} - \mathbf{t}_{\Gamma}) ds. \quad (38)$$

The combination of Eqs. (28) and (37) results in finite-element formulations for each element:

$$\begin{bmatrix} \mathbf{F} - \omega^2 \mathbf{M} - \mathbf{A} \\ -\mathbf{A}^t \end{bmatrix} \begin{Bmatrix} \mathbf{p} \\ \mathbf{q} \end{Bmatrix} = \begin{Bmatrix} \mathbf{e} \\ \mathbf{v} \end{Bmatrix}. \quad (39)$$

The governing system of the structure discretized into elements is obtained by assembling the elementary system (39) in terms of the same displacement law on boundaries shared by adjacent elements. The resulting governing system, which is sparse and symmetric, is formally identical to the elementary system (39).

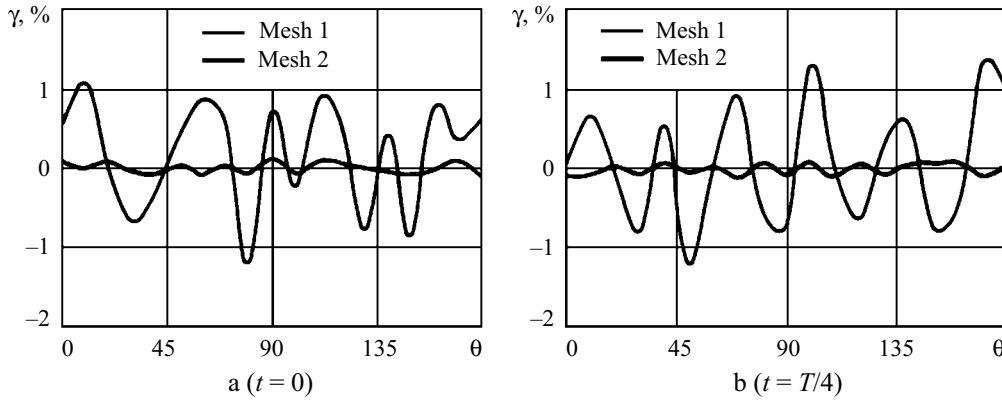


Fig 5. Distributions of the relative errors of the principal stresses for $k_1a = 1.5$

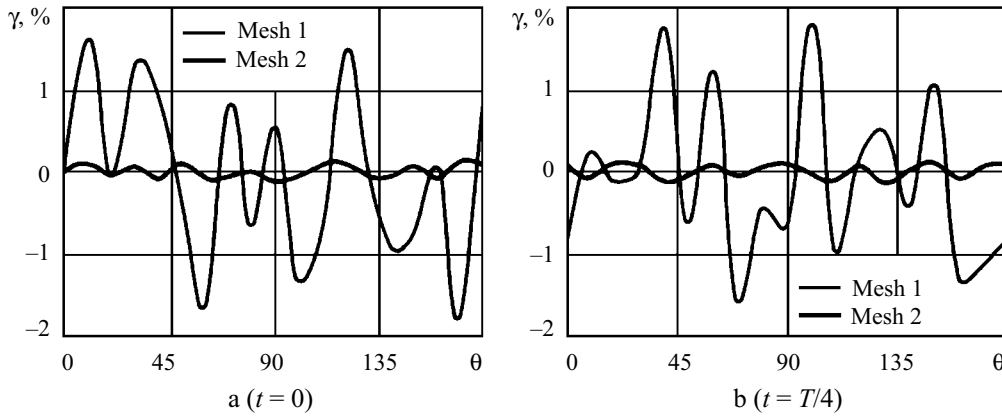


Fig. 6. Distributions of the relative errors of the principal stresses for $k_1a = 3.0$

It is common in the development of hybrid/mixed elements to condense the elementary system (39) into a reduced number of degrees of freedom used for conforming nodal displacement fields before assembling. However, the resulting governing system used here is directly set up from the elementary system (39) and solved by using a sufficient code suitable for large sparse systems, which result from the hierarchic approximation functions implemented in the meshes of few but very rich elements.

5. Numerical Applications.

5.1. Scattering at a Circular Cavity in an Infinite Plate. Figure 3 shows an infinite plate with a circular cavity of diameter a . The plate has Poisson's ratio $\nu = 0.35$. A plane compressional wave $\phi_{\text{inc}}(\Omega, t) = e^{i(k_1x - \omega t)}$ is incident on the plate. When compressional waves encounter the boundary of the cavity, reflected waves are generated.

Figure 4 shows two regular finite-element meshes 1×6 and 3×18 inside the artificial circle whose diameter is $8a$. Polynomials of the second and third degrees are used to implement the domain stresses, $d_\sigma = 3$, and the boundary displacements, $d_u = 2$, in approximations (14) and (15), respectively. This configuration includes 30 degrees of freedom for stresses in each finite element and six degrees of freedom for displacements in each boundary element. Since $\tau_{r\theta} = 0$ at $r = a$, $\tau_{rr} = 0$ and $\tau_{\theta\theta}$ are the principal stresses. The relative errors of the principal stresses γ are defined as $\gamma = (\sigma_{\theta\theta FE} - \sigma_{\theta\theta \text{exact}}) / \max(\sigma_{\theta\theta \text{exact}})$. Figures 5 and 6 show the distributions of the relative errors of the principal stresses at the boundary $r = a$ for $k_1a = 1.5$ and $k_1a = 3.0$, respectively. Two instants of time are considered: $t = 0$ and $t = T/4$, where $T = 2\pi / \omega$ is the period of the incident wave. Since the stresses are symmetric about $\theta = 0$, only half the distribution is shown. The finite element results are compared with the analytic solutions presented by Pao [27]. From Fig. 5 it can be concluded that for $k_1a = 1.5$ an analysis with only six elements results in the maximum errors of about 1.2%, and the maximum errors with 18 elements are within 0.09%. In Fig. 6, the maximum errors for six and 18 elements are within 1.8% and 0.12%, respectively.

For harmonic waves, the average energy flux per unit area is defined by $e_k - 1/4i\omega(\tau_{kl}u_l^* - \tau_{kl}^*u_l)$ and the scattering cross section by the ratio of the flux of scattered fields through a surface of radius r to the average incident energy flux:

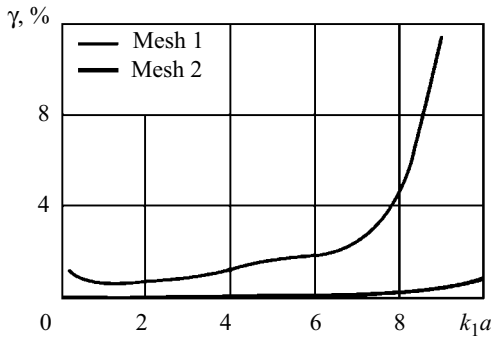


Fig. 7. Relative errors of the scattering cross section

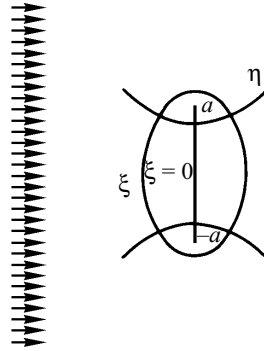


Fig. 8. Plane wave incident on a cavity ribbon

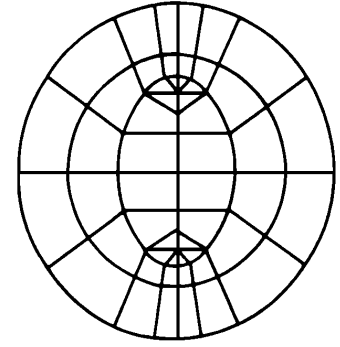


Fig. 9. Hybrid finite element mesh

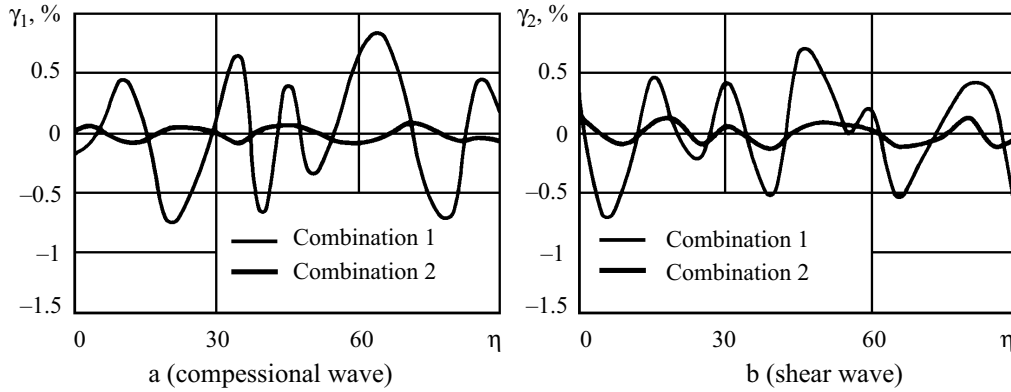


Fig. 10. Distributions of the relative errors of scattered waves for $k_1a = 1.0$

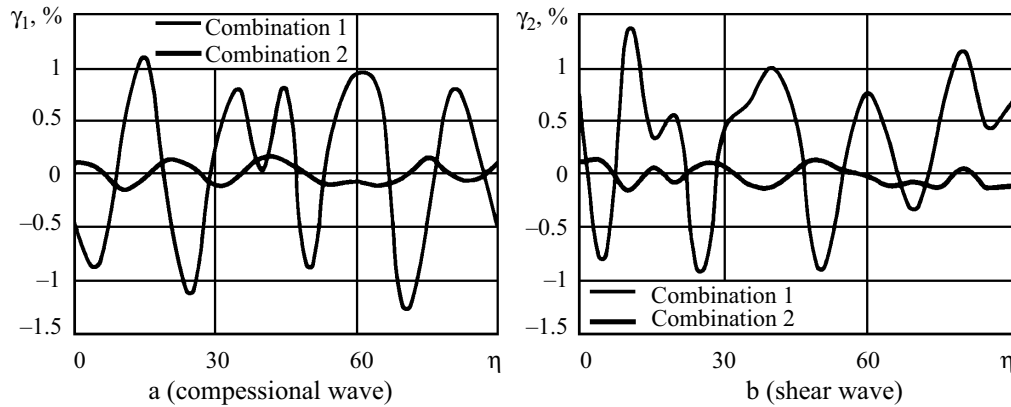


Fig. 11. Distributions of the relative errors of scattered waves for $k_1a = 3.0$

$\bar{e} = \left(\int_0^{2\pi} e_r r d\theta \right) / e_0$. The relative errors of the scattering cross section are defined as $\gamma_0 = |\bar{e}_{FE} - \bar{e}_{\text{exact}}| / \bar{e}_{\text{exact}}$. Figure 7 shows the relations between the relative errors of the scattering cross section and the normalized wave number k_1a . The curve for 18 elements is very smooth, and the maximum relative error is 0.7% at $k_1a = 10.0$. The relative errors for six elements are 1.5% when $k_1a = 6.0$. However, the relative error for six elements is 11% at $k_1a = 9.0$, i.e., this mesh is too coarse for large values of the normalized wave number k_1a .

5.2. Scattering of Plane Waves by a Cavity Ribbon in a Solid. Figure 8 shows plane incident waves scattered by a cavity ribbon of width $2a$ in an elastic medium with Poisson's ratio $\nu = 1/3$. The incident plane compressional wave $\phi_{\text{inc}}(\Omega, t) = (i/k_1)e^{i(k_1x - \omega t)}$ is perpendicular to the axis of the cavity ribbon.

TABLE 1

$k_1 a$	Combination 1 (%)	Combination 2 (%)
1.0	0.45	0.08
3.0	0.63	0.11

The problem is solved with a fifty-two-element mesh inside the artificial circle shown in Fig. 9. The p -convergence procedure is implemented by using two combinations. One is $(d_v, d_\Gamma) = (2, 1)$, which means using polynomials of the second and third degrees in (14) and (15), respectively. The other combination is $(d_v, d_\Gamma) = (4, 3)$, which results in 45 degrees of freedom for the stresses in each finite element and eight degrees of freedom for the displacements in each boundary element. Harumi [28] represented the far-field distributions of displacement within an angle $f(\eta)$ for scattered compressional waves and within an angle $g(\eta)$ for scattered shearing waves as $u_\xi = -ir^{-1/2} e^{ik_1 r} f(\eta)$ and $u_\eta = ir^{-1/2} e^{ik_2 r} g(\eta)$. The finite-element results are evaluated by defining the relative errors:

$$\gamma_1 = \frac{f_{FE} - f_{\text{exact}}}{\max(f_{\text{exact}})} \text{ and } \gamma_2 = \frac{g_{FE} - g_{\text{exact}}}{\max(g_{\text{exact}})}.$$

The angular distributions of the relative errors for scattered compressional and shear waves are shown in Fig. 10 and 11 for $k_1 a = 1.0$ and $k_1 a = 3.0$, respectively. It may be seen that the maximum relative errors for compressional and shear waves under combination 1 are 0.8% and 0.7%, respectively, in Fig. 10 and 1.3% and 1.4%, respectively, in Fig. 11. For combination 2, the maximum relative errors are within 0.2% in both Figs. 10 and 11.

The results summarized in Table 1 are the relative errors for scattering cross sections per unit length of the ribbon for the incident waves. It may be seen that the maximums relative errors are 0.63% and 0.11% for the two combinations, respectively.

6. Conclusions. The above applications of the hybrid equilibrium finite elements to the wave diffraction problems result in the following conclusions: The resulting governing system is sparse and symmetrical and, if well done, can be free of spurious modes [29]. The system is particularly well suited to parallel processing because it is based on relatively coarse meshes of hierarchical finite elements, which lead to finite element variables that are strongly element-dependent. As the Hankel function is still used as the approximation bases in the far field, the formulations for far-field analyses, such as the scattering cross section for wave diffraction problems, are similar to those used with analytic solutions. The numerical results indicate that the rates of convergence, both in h - and p -refinements, are high and that good levels of accuracy are obtained in the estimates of stresses and displacements. Since problem-independent, the finite-element formulations can be extended to dynamic analyses of bending plates.

REFERENCES

1. P. Bettess, "Infinite elements," *Int. J. Numer. Meth. Eng.*, **11**, 53–64 (1977).
2. O. C. Zienkiewicz, K. Bando, P. Bettess, C. Emson, and T. C. Chiam, "Mapped infinite elements for exterior wave problems," *Int. J. Numer. Meth. Eng.*, **21**, 1229–1251 (1985).
3. R. J. Astly and W. Eversman, "A note on the utility of a wave envelope approach in finite element duct transmission studies," *J. Sound Vib.*, **76**, 595–601 (1981).
4. L. Cremers and K. R. Fyfe, "On the use of variable order infinite wave envelope elements for acoustic radiation and scattering," *J. Acoust. Soc. Amer.*, **97**, 2028–2040 (1995).
5. J. A. Bettess and P. Bettess, "A new mapped infinite wave element for general wave diffraction problems and its validation on the ellipse diffraction problem," *Comput. Meth. Appl. Mech. Eng.*, **164**, 17–48 (1998).

6. H. A. Schenck, "Improved integral formulation for acoustic radiation problems," *J. Acoust. Soc. Amer.*, **44**, 41–58 (1968).
7. W. L. Meyer, W. A. Bell, B. T. Zinn, and M. P. Stallybrass, "Boundary integral solutions of three dimensional acoustics radiation problems," *J. Acoust. Soc. Amer.*, **59**, 245–262 (1978).
8. V. Rokhlin, "Rapid solution of integral equations of scattering theory in two dimensions," *J. Comp. Phys.*, **86**, 414–439(1990).
9. X. Zeng and J. Bielak, "Exterior stable domain segmentation integral equation method for scattering problems," *Int. J. Numer. Meth. Eng.*, **37**, 777–792 (1994).
10. T. H. H. Pian, "Derivation of element stiffness matrices by assumed stress distribution," *J. AIAA*, **2**, 1333–1335(1964).
11. T. H. H. Pian and P. Tong, "Basis of finite element methods for solid continua," *Int. J. Numer. Meth. Eng.*, **1**, 3–28(1969).
12. S. N. Atluri, "A new assumed stress hybrid finite element model for solid continua," *J. AIAA*, **9**, 1647–1649 (1971).
13. R. D. Cook and S. G. Laskany, "Observations regarding assumed stress hybrid plate element," *Int. J. Numer. Meth. Eng.*, **8**, 513–520 (1974).
14. J. Jirousek and A. Wroblewski, "T-elements: State of the art and future trends," *Arch. Comput. Meth. Eng.*, **3**, 323–434 (1996).
15. J. P. M. Almeida and O. J. B. A. Pereira, "A set of hybrid equilibrium finite element models for the analysis of three-dimensional solid," *Int. J. Numer. Meth. Eng.*, **39**, 2789–2802 (1996).
16. J. A. T. Freitas and Z. Y. Ji, "Hybrid Trefftz equilibrium model for crack problems," *Int. J. Numer. Meth. Eng.*, **39**, 569–584(1996).
17. J. A. T. Freitas and Z. M. Wang, "Hybrid Trefftz stress elements for elastoplasticity," *Int. J. Numer. Meth. Eng.*, **43**, 655–683 (1998).
18. O. J. B. A. Pereira, J. P. M. Almeida, and E. A. W. Maunder, "Adaptive methods for hybrid equilibrium finite element models," *Comput. Meth. Appl. Mech. Eng.*, **176**, 19–39(1999).
19. J. A. T. Freitas, "Hybrid finite element formulations for elastodynamic analysis in the frequency domain," *Int. J. Solids Struct.*, **36**, 1883–1923 (1999).
20. J. A. T. Freitas and Z. M. Wang, "Elastodynamic analysis with hybrid stress finite elements," *submitted for publication*, 2000.
21. J. A. T. Freitas and Z. M. Wang, "Elastoplastic dynamic analysis with hybrid stress finite elements," *submitted for publication*, 2000.
22. Ya. M. Grigorenko and S. S. Kokoshin, "Design of shell structures by the finite-element method," *Sov. Appl. Mech.*, **15**, No. 7, 567–573 (1979).
23. Ya. M. Grigorenko and S. S. Kokoshin, "Numerical analysis of state of stress of multilayer anisotropic shells according to hybrid model of finite elements," *Sov. Appl. Mech.*, **18**, No. 2, 89–92 (1982).
24. V. G. Piskunov and A. O. Rasskazov, "Evolution of the theory of laminated plates and shells," *Int. Appl. Mech.*, **38**, No. 2, 135–166 (2002).
25. I. I. Vorovich and L. P. Lebedev, "Some issues of continuum mechanics and mathematical problems in the theory of thin-walled structures," *Int. Appl. Mech.*, **38**, No. 4, 387–398 (2002).
26. V. A. Bazhenov, A. S. Sakharov, and V. K. Tsykhanovskii, "The moment finite-element scheme in problems of nonlinear continuum mechanics," *Int. Appl. Mech.*, **38**, No. 6, 658–692 (2002).
27. Y. H. Pao, "Dynamic stress concentration in an elastic plate," *J. Appl. Mech.*, **29**, 299–305 (1962).
28. K. Harumi, "Scattering of plane waves by a cavity ribbon in a solid," *J. Appl. Phys.*, **33**, 3588–3593 (1962).
29. E. A. W. Maunder and J. P. M. Almeida, "Hybrid-equilibrium elements with control of spurious kinematic modes," *GAMES*, **4**, 587–605(1996).

Copyright of International Applied Mechanics is the property of Kluwer Academic Publishing / Academic and its content may not be copied or emailed to multiple sites or posted to a listserv without the copyright holder's express written permission. However, users may print, download, or email articles for individual use.